Structural Analysis of the Protein/Lipid Complexes Associated with Pore Formation by the Bacterial Toxin Pneumolysin*

Boyan B. Bonev‡, Robert J. C. Gilbert‡§¶, Peter W. Andrew§, Olwyn Byron‖, and Anthony Watts‡

From the ‡Biomembrane Structure Unit, Department of Biochemistry, University of Oxford, South Parks Road, Oxford OX1 3QU, the §Department of Microbiology and Immunology, University of Leicester, Leicester LE1 9HN, and the ‖Institute of Biomedical and Life Sciences, Division Infection and Immunity, University of Glasgow, Glasgow G12 8QQ, United Kingdom

Pneumolysin, a major virulence factor of the human pathogen *Streptococcus pneumoniae*, is a soluble protein that disrupts cholesterol-containing membranes of cells by forming ring-shaped oligomers. Magic angle spinning and wideline static ^{31}P NMR have been used in combination with freeze-fracture electron microscopy to investigate the effect of pneumolysin on fully hydrated model membranes containing cholesterol and phosphatidylcholine and dicetyl phosphate (10:10:1 molar ratio). NMR spectra show that the interaction of pneumolysin with cholesterol-containing liposomes results in the formation of a nonbilayer phospholipid phase and vesicle aggregation. The amount of the nonbilayer phase increases with increasing protein concentration. Freeze-fracture electron microscopy indicates the coexistence of aggregated vesicles and free ring-shaped structures in the presence of pneumolysin. On the basis of their size and analysis of the NMR spectra it is concluded that the rings are pneumolysin oligomers (containing 30–50 monomers) complexed with lipid (each with 840–1400 lipids). The lifetime of the phospholipid in either bilayer-associated complexes or free pneumolysin-lipid complexes is > 15 ms. It is further concluded that the effect of pneumolysin on lipid membranes is a complex combination of pore formation within the bilayer, extraction of lipid into free oligomeric complexes, aggregation and fusion of liposomes, and the destabilization of membranes leading to formation of small vesicles.

Pneumolysin is a major virulence factor from the human pathogen *Steptococcus pneumoniae* and is a member of a family of cholesterol-binding toxins (CBTs),[1] which also includes per-

fringolysin from *Clostridium perfringens*, listeriolysin from *Listeria monocytogenes,* and streptolysin from *Streptococcus pyogenes*. Streptolysin is well known for its use in cell biology for the permeabilization of cells. As well as pore formation leading to the breakdown of membrane barriers into cells and between tissues, these toxins act in a complex manner involving the activation of intracellular signaling pathways and the induction of inflammation, among other responses (see Morgan *et al.* (1) for review). Understanding the mechanisms by which CBTs act has been greatly assisted by the determination of a crystal structure for soluble, monomeric perfringolysin (2) and the use of electron cryo-microscopy (cryo-EM) to obtain three-dimensional reconstructions of the oligomeric and pore-forming states of CBTs using pneumolysin (3). These direct structural insights have been augmented by results obtained by Tweten and co-workers (4) using fluorescence spectroscopy (5), which demonstrate that a pendant domain of the CBTs interacts with phospholipid molecules during pore formation via two α-helix bundles refolded into two β-hairpins. A second terminal domain is known to be involved in membrane binding via cholesterol. Thus, it seems that the CBT mechanism involves two domains interacting with the membrane (6, 3).

Two mechanisms for pneumolysin action in disease are well defined (7). First, pneumolysin is well known as a pore-forming toxin that binds to cholesterol in membranes, oligomerizes into ring-shaped assemblies, and undergoes conformational changes causing it to penetrate and form a pore within the bilayer (3). Secondly, pneumolysin activates the complement system in a nonimmunospecific manner as a result of interaction with IgG-Fc and complement proteins (8, 9).

Solid state NMR provides a direct and quantitative way for investigating lipid-protein interactions in membranes (10–12). Changes in protein-induced phospholipid phase behavior can be observed through characteristic intensity distribution in the chemical shift anisotropy (CSA)-dominated lineshapes of wideline ^{31}P NMR spectra. Characteristic lineshapes have been observed from phospholipid phases with different modes of molecular motions (Fig. 1 and Refs. 13–15). Using ^{31}P magic angle spinning (MAS) NMR, the individual lipid components in the bilayer can be resolved (11), and changes in their isotropic chemical shift, CSA and full-width at half-height (FWHH) in response to modulation of the phosphate motions in the presence of proteins determined (11, 12, 16).

Here results from solid-state NMR and electron microscopy are presented that provide novel insights into the mechanism of CBTs and complement data already acquired using other

---

¶ Present address: Division of Structural Biology, Wellcome Trust Centre for Human Genetics, University of Oxford, Roosevelt Dr., Oxford OX3 7BN, UK.

** A BBSRC Senior Research Fellow. To whom correspondence should be addressed. Tel.: 44 1865 275 268; Fax: 44 1865 275 234; E-mail: awatts@bioch.ox.ac.uk.
[1] The abbreviations used are: CBT, cholesterol-binding toxin; MAS, magic angle spinning; FWHH, full width at half-height; CS (σ), isotropic chemical shift; σ_p and σ_f, chemical shift of the toxin-dependent and the toxin-free phospholipid environment; CSA, chemical shift anisotropy; EM, electron microscopy; LUV, large unilamellar vesicle; MLV, multilamellar vesicle; τ_{ex}^{-1}, rate of lipid exchange between different phases

or environments; τ_R^{-1}, rate of rotational motion; PC, phosphatidylcholine; DCP, dicetylphosphate.

techniques. Suspensions of cholesterol-containing liposomes are a model system that has already been used for analysis of pore formation by pneumolysin using small-angle neutron scattering (9) and cryo-EM (3).

MATERIALS AND METHODS

Sample Preparation—Large unilamellar vesicles (LUVs) of egg-yolk phosphatidylcholine (PC), cholesterol, and dicetylphosphate (DCP) in a 10:10:1 molar ratio were prepared in 100 mM Tris buffer, pH 7.5, at 5 mM concentration as previously described (3). Multilamellar vesicles (MLVs) used in a control experiment were prepared by five cycles of rapid freezing of hydrated lipid mixtures followed by 15 min equilibration at 40 °C. Pneumolysin was expressed from recombinant *Escherichia coli* and purified as previously described (17). Pneumolysin was mixed with liposomes at a variety of molar ratios to cholesterol and incubated at 37 °C for 10 min prior to data acquisition.

NMR Spectroscopy—Phosphorus-31 wideline and MAS NMR measurements were carried out on a CMX Infinity 500 spectrometer at a proton frequency of 500 MHz. Typically 5 μmol of lipid dispersion were used in a 4-mm rotor using an HX Apex probe. A single 90° pulse was used for detection with broadband decoupling at the proton frequency during acquisition. The 90° pulse length was 4 μs, and the strength of the proton decoupling field was 20 kHz. The dwell time used was 40 μs, and 2048 points were collected in each experiment. Between 300 and 3000 transients were averaged for each free induction decay (FID) during MAS experiments and between 5000 and 10,000 during wideline experiments with a 5-s delay (exceeding $5T_1$) between acquisitions in all cases. The sample rotation speed was maintained at 12 kHz during acquisition of the MAS spectra, and the temperature was set to 30 °C for all experiments.

High speed MAS lineshape analysis was performed by fitting simulated Lorentzian lines to the experimental spectra using Spinsight (Chemagnetics, Fort Collins, CO) and Felix (MSI, Cambridge). The intensity of the individual lines was estimated from the integral of the simulated spectra. All ^{31}P chemical shifts are measured relative to 0 ppm for 10% v/v phosphoric acid. All spectra were obtained with 50 Hz linebroadening for the wideline spectra and 10 Hz for the MAS spectra.

Electron Microscopy—Samples of LUV suspensions from NMR experiments were prepared for freeze-fracture by equilibration at room temperature, followed by a rapid immersion into liquid butane at its solidification point (18). Fracture of the immobilized frozen droplets was performed at −100 °C, followed by platinum shadowing at 45° with respect to the fractured surface and a normal deposition of a uniform carbon film in a Balzers freeze-etching apparatus. Residual sample was removed from the carbon-platinum replicas by cyclic exposure to potassium hypochlorate and methanol. The carbon-platinum replicas were transferred onto copper electron microscope grids. A Phillips CM120 transmission electron microscope was used for grid visualization at 100-kV accelerating voltage and 45,000 × magnification.

RESULTS

Lipid Dynamics and Phase Behavior-Phosphorus-31 Wideline NMR—Wideline ^{31}P NMR was used to monitor changes in the phospholipid phase behavior induced by the addition of pneumolysin. LUVs of egg yolk PC, cholesterol, and DCP (molar ratio 10:10:1) were incubated with pneumolysin at 30 °C. Spectra from the lipid vesicles alone (see Fig. 2a) and in the presence of pneumolysin at different concentrations are shown (Fig. 2, *b–d*). The ^{31}P NMR spectrum from lipid suspension prior to addition of pneumolysin (Fig. 2a) consists of a single narrow line. The collapse of the phosphorus CSA is because of fast rotation of relatively small (<100 nm in diameter) unilamellar vesicles (19). The correlation times (τ_R) for tumbling of such vesicles are on the order of 10^{-4}–10^{-5} s, which exceeds the inverse width of the average ^{31}P CSA (~40–50 ppm, ~6 kHz) for lipid phosphates in extended bilayers.

Fig. 2b shows the spectrum from the phospholipid dispersion after addition of pneumolysin at 0.5 mol % with respect to cholesterol. The spectrum is characteristic of a ^{31}P CSA-dominated spherically averaged (powder) pattern (20) from phospholipid bilayers in extended structures of average size greatly exceeding 100 nm. The most likely cause of this change in apparent liposome size when compared with protein-free lipo-
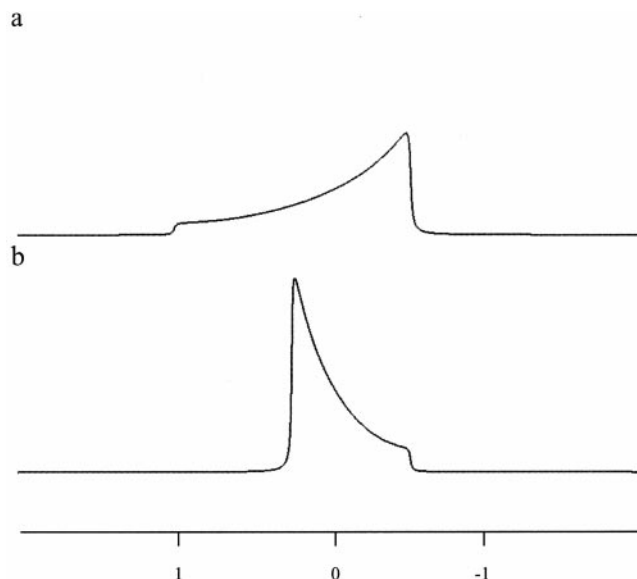

FIG. 1. **Simulated characteristic lineshapes from spherically symmetric lipid distribution (bilayer phase, *a*) and cylindrically symmetric lipid distribution (H_{II} phase, *b*) with the same effective CSA.** Lineshapes were simulated using Maple 6 (University of Waterloo, Canada).
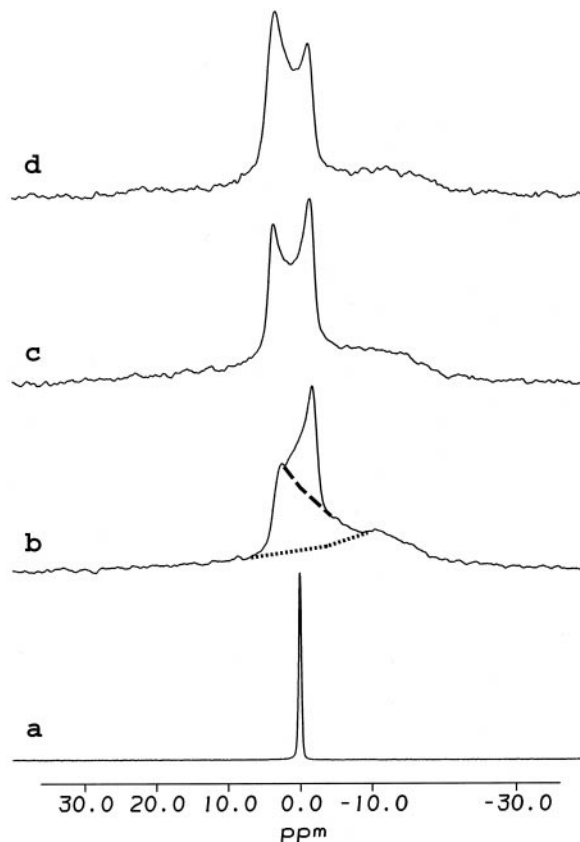

FIG. 2. **Wideline ^{31}P NMR spectra from egg PC/cholesterol/DCP LUV dispersions in a molar ratio of 10:10:1 (*a*) and after addition of 0.5 mol % (*b*), 1.25 mol % (*c*), and 1.5 mol % (*d*) pneumolysin.** A *dotted* and a *dashed line* are added to the spectrum in *b* to identify the spectral contribution from the bilayer PC (*below dotted line*), nonbilayer lipid (*between dotted* and *dashed lines*), and bilayer DCP (*above dashed line*). See text for details.

somes (Fig. 2a) is vesicle aggregation induced by the interaction of toxin with the membranes. The motional properties of these complexes indicate that the average size of the lipid aggregates exceeds 1 μm because their reorientation rate
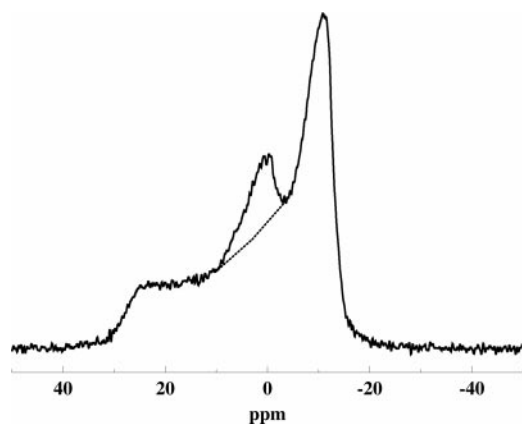
FIG. 3. **Wideline ^{31}P NMR spectrum from an egg PC/cholesterol/DCP MLV dispersion in a molar ratio of 10:10:1.** The *dotted lines* help distinguish the PC powder pattern (*bottom*) from the DCP powder pattern (*top*).

FIG. 4. **Phosphorus-31 MAS NMR spectra from egg PC/cholesterol/DCP LUV dispersions in a molar ratio of 10:10:1 (*a*) and after addition of 0.5 mol % (*b*), 1.25 mol % (*c*), and 1.5 mol % (*d*) pneumolysin.** See text for details.

(τ_R^{-1}) is much lower than 6 kHz (the effective CSA of lipid phosphates). The spectrum of Fig. 2*b* reveals three overlapping features, a powder pattern between $\sim$27 and -14 ppm (*below dotted line*), a second powder pattern with reduced effective CSA from 5 to -2 ppm (*above dashed line*), and an inverted powder-like distribution from 3 to about -8 ppm (Fig. 2, *between dotted* and *dashed lines*, see characteristic lineshapes). The two powder patterns arise from a spherical distribution of lipid molecules rapidly rotating about their long axes. The downfield intense feature in the powder patterns corresponds to molecules oriented at 90 degrees with respect to the external magnetic field and the upfield distribution of intensity to molecules oriented along the field. The width of the broader powder pattern (*below dotted line*) is characteristic of phosphatidylcholine aggregates undergoing slow reorientation and is likely to result from liposomes aggregated in the presence of pneumolysin. The narrow powder pattern (*above dashed line*) is generated by the phosphates of DCP in the same lipid bilayer. These powder distributions can be observed as a result of the interaction between the vesicles in the presence of pneumolysin. The relative intensity of the powder patterns with respect to each other is independent of the amount of toxin added to the lipid suspension (Fig. 2, *b–d*), which suggests that the PC/DCP ratio in the bilayer remains constant. In a control experiment, an MLV (large complexes with $\tau_R^{-1} \gg$ effective CSA) suspension produced a wideline ^{31}P NMR spectrum (Fig. 3) consisting of two powder patterns of comparable relative intensity and of similar effective CSA to the powder patterns observed in the presence of pneumolysin (Fig. 2).

The inverted powder-like feature of Fig. 2*b* is characterized by a sharp upfield edge, arising from molecules oriented at 90 degrees with respect to the external field and a downfield extended region from lipids oriented along the magnetic field. Inverted powder-like patterns arise from nonbilayer lipid complexes with cylindrical symmetry of motion like, for example, the lipid tubular structures in inverted hexagonal (H$_{II}$) phases (14). The effective CSA, measured from these patterns ($\sim$11 ppm), is less than the expected half-spectral width from the bilayer environment ($\sim$40 ppm) and exceeds the measured effective CSA of the narrow powder pattern (associated with the presence of DCP). This suggests that fast rotation of the phospholipid aggregates in the axially symmetric environment results in additional reduction in the effective CSA and excludes the possibility of formation of a cylindrically symmetric lipid distribution from the lipid environment with small effective CSA by a simple reduction of spherical to cylindrical symmetry. In the latter case, the width of the axially symmetric
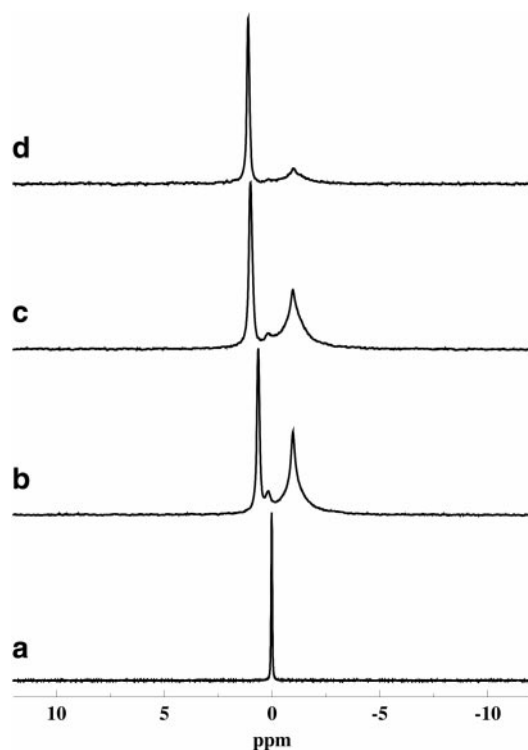
distribution would be derived as a half of the effective CSA in the related spherical distribution (14, 15).

Further increase in the pneumolysin concentration results in a relative increase in the intensity of the cylindrical lipid distribution and a decrease in the intensity of both powder patterns (Fig. 2, *c* and *d*). This behavior shows that the cylindrical lipid population arises from a pneumolysin-associated lipid environment. The good spectral definition of the characteristic edges of the lipid environments indicates well separated phases with none or with very slow ($\tau_{ex}^{-1} < 200$ Hz), lipid exchange between them. The 90° edges from the different lipid environments remain at the same chemical shift, which suggests that the effective CSA and, therefore, the motional characteristics of these environments are independent of pneumolysin concentration.

Quantification of the Pneumolysin-Lipid Interaction by Phosphorus-31 MAS NMR—Phosphorus-31 MAS NMR is used here as a high-resolution approach to membrane studies for quantitative characterization of the different phospholipid environments (11). High speed MAS ^{31}P NMR spectra from different lipid-pneumolysin mixtures are shown in Fig. 4. The lipid suspension in the absence of toxin gives rise to a single resonance at $\sim$0 ppm. The observed unusual chemical shift of the resonance line and the lack of resolution between PC and DCP are most likely because of an interference of the vesicle tumbling and lateral diffusion of the phospholipid molecules with the proton-phosphorus decoupling and MAS. Such interaction may result in inefficient proton decoupling and incomplete averaging of the ^{31}P CSA under MAS for 100 nm LUVs (see Ref. 21 for discussion). In a control ^{31}P MAS NMR experiment an MLV suspension of the same composition produced a strong resonance at approximately -1.0 ppm, attributed to the PC phosphate and a weak resonance at 0.1 ppm from DCP (spectrum not shown).

All ^{31}P MAS NMR spectra in the presence of pneumolysin

Phosphorous-31 isotropic chemical shifts (σ_p, σ_f) from MAS NMR of the non-bilayer and total bilayer lipid resonance and relative intensity I as a fraction of the total spectral intensity determined from the spectra in Fig. 2 for different concentrations of pneumolysin with respect to cholesterol at 30 °C are shown.

Pneumolysin	$\sigma_p{}^a$	σ_f	I_p	I_f
mol %	*ppm*	*ppm*	*%*	*%*
0.00	0.00	0.00	0	100
0.50	0.65	−1.04	32	68
1.25	1.01	−1.05	40	60
1.50	1.12	−1.05	60	40

[a] Bilayer lipid is in LUVs and not in the extended bilayers.

show two distinctive resonances, (Fig. 4, *b–d*), a downfield one at approximately −1.0 ppm and an upfield resonance with chemical shift dependent on the pneumolysin concentration (Table I). The resonance at −1.0 ppm has the characteristic chemical shift of phosphatidylcholine in a bilayer environment (11) and consists of two overlapping resonances, one of FWHH approximately equal to 1.61 ppm and another of 0.35 ppm FWHH. The FWHH of the broader resonance increases at higher pneumolysin concentration, whereas that of the narrower resonance does not show a clear dependence on toxin concentration. The broader resonance, therefore, probably arises from pneumolysin-associated lipid within the lipid bilayer phase in the form of pores (see EM evidence below) or between partially fused liposomes. A low intensity resonance at 0.1 ppm arises from DCP in the bilayer. The ratio between its intensity and the intensity of the PC at −1.0 ppm resonance does not depend on pneumolysin concentration.

The narrow upfield resonance (Fig. 4*b*) undergoes a pronounced further upfield change in its isotropic chemical shift, σ, with increasing pneumolysin concentration (Table I). The relative intensity of this resonance when compared with the total intensity of the line at −1.0 ppm increases as the toxin concentration is increased (Table I). The toxin concentration-dependent increase in the intensity of this resonance parallels, in a qualitative way, the increase in the intensity of the reverse powder pattern, observed in the static spectra (Fig. 2, *b–d*). Therefore, the upfield resonance most likely arises from lipid associated with pneumolysin in the nonbilayer environment.

Morphology of the Lipid Phases by Freeze-Fracture EM— Freeze-fracture electron microscopy was used to obtain information about the lipid phase topology in the presence of pneumolysin. Fig. 5 shows transmission electron micrographs from the lipid system in the presence of 1.25 mol % pneumolysin with respect to cholesterol. The micrographs show aggregated lipid vesicles, with the vesicles varying in size from one hundred to a few hundred nanometers. Fractures across the vesicles reveal single or only a few bilayers and thus the absence of multibilayer structures. Nonaggregated vesicles are also seen in coexistence with the vesicle aggregates. Multifaceted liposome surfaces reveal close foam-like aggregation. The surfaces of some liposomes show the presence of circular structures of ~25 nm internal diameter (Fig. 5*a, arrow p*). Previously observed pneumolysin oligomers have a similar size to these circular structures and represent, most likely, membrane-incorporated oligomeric toxin pores (3).

Free ring-shaped structures unassociated with liposomes are also observed with an inside diameter of ~25 nm and an outside diameter of about 50 nm (Fig. 5*a, arrow r*). These appear to be the only axially symmetric structures in the system and are the same size as the rings seen here on liposomes, and previously on liposomes in solution (3). Fig. 5*b* (*arrow*) shows a structure of the same size (~25-nm inner diameter) as

the rings of Fig. 5*a*, localized at the boundary between two liposomes having a common wall. This suggests that pneumolysin oligomers play a role in liposome aggregation and fusion. A lipid environment resembling that in the proteolipid rings is associated with the pneumolysin ring shown in Fig. 5*b*. This suggests that vesicle aggregation may be related to the formation of nonbilayer proteolipid structures.

DISCUSSION

An important aspect of the effect of pneumolysin on membranes is the destabilizing effect the protein has on the lipid bilayers and the associated withdrawal of phospholipids into nonbilayer structures. The wideline ^{31}P NMR spectra (Fig. 2, *b–d*) originate from a coexistence of phospholipids in structures with a spherically averaged CSA corresponding to the CSA of slowly tumbling MLV's, together with a nonbilayer phase with axially symmetric motion of the lipid structures. The changes in intensity distribution from a powder, to a distribution with the 90° edge located upfield with respect to the 0° extreme, are indicative of the presence of an additional axis of phospholipid molecular averaging, perpendicular to the main axis of lipid rotation. This situation is observed, for example, in the presence of inverted hexagonal (H_{II}) phases (15, 22). In addition to the inversion of spectral intensity distribution, the overall width of the CSA-dominated intensity distribution is expected to decrease by a factor of 2 (see Fig. 1 and Refs. 13, 15). The width of the spectrum from the pneumolysin-induced nonbilayer phase (~10 ppm) is reduced further to ~one-fourth of the spectral width from the lipid powder distribution (~40 ppm). This suggests the presence of fast axial rotation of the lipids in these structures and that they are smaller than the average diameter of a lipid aggregate in an H_{II} phase. The increase in the fraction of the nonbilayer phase with increasing toxin concentration strongly indicates that its formation is induced by pneumolysin (Fig. 2, *b–d*).

The ring structures, shown in the micrographs in Fig. 5 possess all the characteristics necessary to give rise to the inverted powder component in the static ^{31}P NMR spectra of Fig. 2, *b–d*. Their ring shape results in a preferred axis of motional averaging and their relatively small size would facilitate fast axial rotation. The internal diameter of these structures corresponds to the size of pneumolysin rings observed by negative staining EM and cryo-EM (3, 17). The most likely explanation for the rings seen here by EM and detected by a characteristic spectral distribution similar to that of a nonbilayer phase (Fig. 2) is an oligomeric pneumolysin ring with a lipid annulus decorating the exterior of the oligomer (Fig. 6). The interior of such structures could be filled with lipid or empty, because both forms of oligomers have been observed by cryo-EM (3).[2] In either case the evolution of such structures into free solution from liposomes, with which pneumolysin interacts would result in the rapid destruction of the membrane.

The relative intensity of the nonbilayer spectral feature increases in comparison to the intensities of both the wide and the narrow powder patterns. The concomitant increase in the intensity of the upfield resonance in the ^{31}P MAS NMR spectra can be used as a measure of the relative amount of nonbilayer phase (proteolipid rings). Thus the quantitation of spectral intensity (Table I) reflects the fraction of the total lipid, segregated into the rings and indicates that a large proportion of the lipid is associated with free oligomers detached from the lipid bilayer. In particular, the values presented in Table I show that an increase in pneumolysin concentration with respect to cho-

---

[2] R. J. C. Gilbert, J. L. Jimenez, S. Chen, and H. R. Saibil, unpublished results.
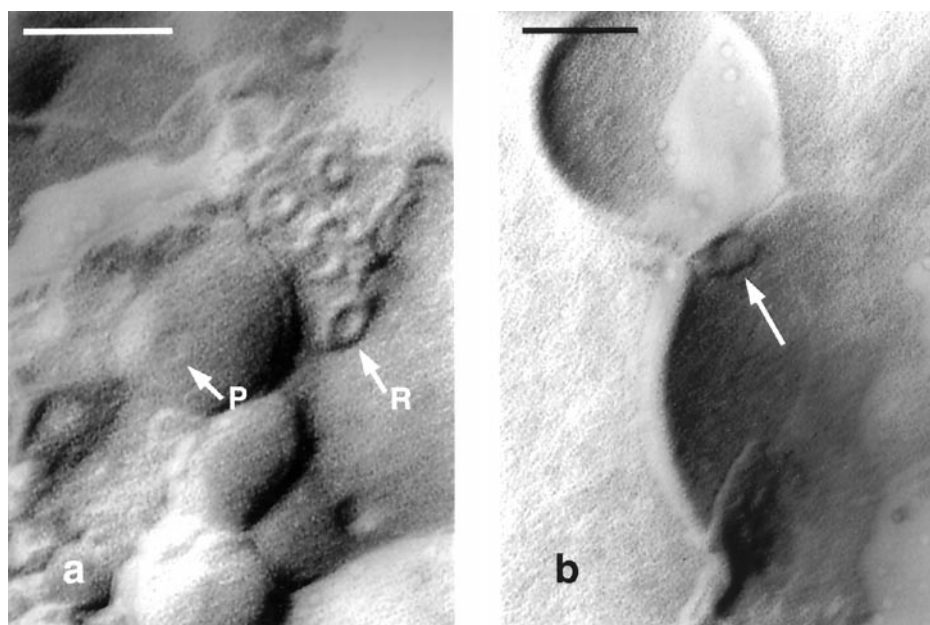
FIG. 5. **Two freeze-fracture electron micrographs (*a, b*) from PC/cholesterol/DCP LUV dispersions in the presence of 1.5 mol % pneumolysin.** The length of the *scale bar* is 100 nm. *Arrow P* shows a membrane pore and *arrow R* shows a proteolipid ring (*a*). The *arrow* in *b* shows a proteolipid structure at the interface of two fused liposomes.
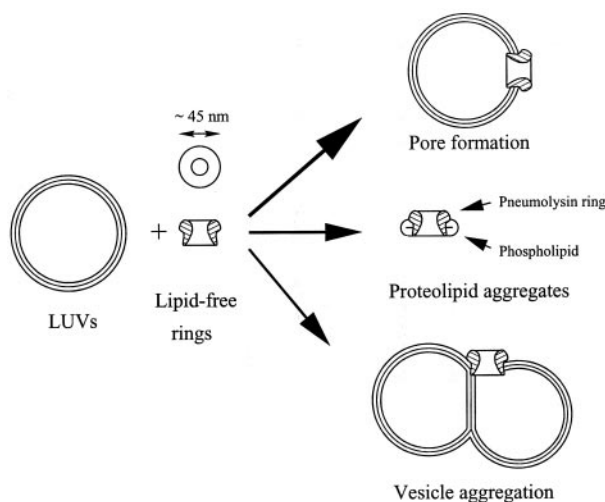

FIG. 6. **Schematic illustration of the effects of pneumolysin on lipid bilayers.** Each oligomer is estimated to be complexed with 840 to 1400 phospholipid molecules. Unilamellar vesicles are ~100 nm in diameter, and the size of the phospholipid aggregate is much greater than 100 nm. Exchange of phospholipid between the structures, if possible, occurs slowly (15 ms).

lesterol from 0.5 to 1.5 mol % results in an increase of nonbilayer phase from 32 to 60% of the total phospholipid content. Consequently, in the presence of ~1 mol % of pneumolysin, 28 phospholipid molecules are associated with each pneumolysin monomer and the number of phospholipid molecules per oligomer, consisting of 30 to 50 toxin molecules (3), can be estimated to vary between 840 and 1400, respectively.

The insights gained here into the mechanism of CBTs are fundamentally important because they suggest that toxin pores do not remain associated with bilayer membranes or bilayer fragments derived from cells, which have been lysed. On the contrary, they become dispersed in complexes with phospholipids and possibly also cholesterol. However, fluorescence studies on the CBT perfringolysin have been interpreted on the premise that the lipids with which the toxin is complexed following pore formation exist in a bilayer environment as part of per-

meabilized membranes (4, 5). Our data suggest that this is not a valid assumption to make and that therefore conclusions on the regions of CBTs that interact with membranes cannot simply be based on fluorescence data, because lipids complexed with CBT oligomers apparently exist in a variety of environments where solid state NMR can be used to distinguish and quantitate in an approximate way.

It is possible to obtain a lower limit for the life-time of the existence of proteolipid rings from the ^{31}P MAS NMR spectra. Two well resolved lines, arising from the two distinct lipid populations, are observed at a CS separation of ~2 ppm (Fig. 4, Table I). The FWHH of the resonance from the nonbilayer environment is ~0.3 ppm. This suggests that any putative exchange of lipid molecules between the bilayer and the nonbilayer lipid environments may occur at a rate much slower than 60 Hz (~1.7 ppm at 500 MHz) or the nonbilayer phase is stable over times exceeding 15 ms.

The freeze-fracture electron micrographs of pneumolysin-containing lipid systems (Fig. 5a) are produced by rapid (~10^4 degrees/second) freezing and reveal the presence of small lipid vesicles derived from the initial suspension, interacting in a toxin-independent fashion with the remaining lipid. These small vesicles appear in the immediate vicinity of the other lipid structures, trapped between larger lipid aggregates, indicating that such toxin-free structures coexist along with other vesicles or liposome-containing toxin. Bearing in mind that the location of these liposomes is within the pneumolysin-induced aggregate, it is reasonable to deduce that they result from the effect of pneumolysin on membranes. The data suggest that the mechanism of pore formation firstly involves oligomerization on or in a bilayer but that later the oligomeric rings enter free solution, withdrawing a large fraction of the lipid membrane into the rings (Fig. 6).

A number of conductance experiments carried out on CBTs indicate that they create pores of a range of sizes and lifetimes in membranes, the smallest of which may be blocked using divalent cations (24). This observation indicates that pores do indeed form within membranes. What our results indicate is that the precise nature of such pores is still uncertain, and may involve lesions formed at the interfaces of nascent oligomeric structures and lipids (25) and discrete protein complexes

within membranes (3) but also large holes in the bilayer alone. Furthermore, effects downstream of oligomerization and pore-formation involving large scale redistribution of membrane components are indicated by our data. It is suggested that the lytic action of pneumolysin on lipid bilayers is a complex combination of pore formation within the membrane, extraction of lipid into free oligomeric complexes, aggregation and fusion of membranes, and membrane destabilization leading to formation of small vesicles. These observations suggest that CBTs may not only permeabilize cell membranes but also cause them to bleb, to aggregate, and to fuse.

The appearance of a large proportion of the lipid and protein as free oligomer-lipid complexes is also important for understanding the noncytolytic mechanisms associated with pneumolysin. As mentioned above, pneumolysin has the ability directly to activate the complement system in a nonimmunospecific manner. This occurs by the classical pathway as a result of the interaction of pneumolysin, IgG-Fc, and complement components (8). Toxin oligomers are known to be capable of complement activation (8), and the existence of large numbers of free oligomers in solution might explain this facility. Although streptolysin has been reported to activate complement in the presence of anti-streptolysin antibodies (26), nonimmunospecific activation of complement has not been demonstrated so far for other CBTs. The oligomers of streptolysin were also found to have a hyperactivating effect on complement compared with monomeric toxin. Such a phenomenon may also occur with pneumolysin, because the domain through which pneumolysin activates complement (the C-terminal domain) has a fold very similar to IgG-Fc, with which it interacts during complement activation (8, 2, 17). IgG itself has a hyperactivating effect on complement when oligomerized (27), which suggests the possibility that the lipids associated with free oligomers may themselves elicit an immune response because nonbilayer (nonplanar) lipid structures have been shown to be highly immunogenic (28). The immunogenicity of such structures is thought to result from their high curvature (28).

REFERENCES

1. Morgan, P. J., Andrew, P. W., and Mitchell, T. J. (1996) *Rev. Med. Microbiol.* **7,** 221–229
2. Rossjohn, J., Feil, S. C., McKinstry, W. J., Tweten, R. K., and Parker, M. W. (1997) *Cell* **89,** 685–692
3. Gilbert, R. J. C., Jiménez, J. L., Chen, S., Tickle, I., Rossjohn, J., Parker, M. W., Andrew, P. W., and Saibil, H. R. (1999) *Cell* **97,** 647–655
4. Shepard, L. A., Heuck, A. P., Hamman, B. D., Rossjohn, J., Parker, M. W., Ryan, K. R., Johnson, A. E., and Tweten, R. K. (1998) *Biochemistry* **37,** 14563–14574
5. Shatursky, O., Heuck, A. P., Shepard, L. A., Rossjohn, J., Parker, M. W., Johnson, A. E., and Tweten, R. K. (1999) *Cell* **99,** 293–299
6. Nakamura, M., Sekino-Suzuki, N., Mitsui, K.-I., and Ohino-Iwashita. (1998) *J. Biochem. (Tokyo)* **123,** 1145–1155
7. Alexander, J. E., Berry, A. M., Paton, J. C., Rubins, J. B., Andrew, P. W., and Mitchell, T. J. (1998) *Microb. Pathog.* **24,** 167–174
8. Mitchell, T. J., Andrew, P. W., Saunders, F. K., Smith, A. N., and Boulnois, G. J. (1991) *Mol. Microbiol.* **5,** 1883–1888
9. Gilbert, R. J. C., Heenan, R. K., Timmins, P. A., Gingles, N. A., Mitchell, T. J., Rowe, A. J., Rossjohn, J., Parker, M. W., Andrew, P. W., and Byron, O. (1999) *J. Mol. Biol.* **293,** 1145–1160
10. Watts, A. (1998) *Biochim. Biophys. Acta* **1376,** 297–318
11. Pinheiro, T. J. T., and Watts, A. (1994) *Biochemistry* **33,** 2459–2467
12. Spooner, P. J. R., and Watts, A. (1992) *Biochemistry* **31,** 10129–10138
13. Seelig, J., and Seelig, A. (1980) *Q. Rev. Biophys.* **13,** 19–61
14. Cullis, P. R., and de Kruijff, B. *(1979) Biochim. Biophys. Acta* **559,** 399–420
15. Yeagle, P. L. (1990) *Biol. Magn. Reson.* **9,** 1–50
16. Carbone, M. A., and Macdonald, P. M. (1996) *Biochemistry* **35,** 3368–3378
17. Gilbert, R. J. C., Rossjohn, J., Parker, M. W., Tweten, R. K., Morgan, P. J., Mitchell, T. J., Errington, N., Rowe, A. J., Andrew, P. W., and Byron, O. (1998) *J. Mol. Biol.* **284,** 1223–1237
18. Severs, N. J., Newman, T. M., and Shotton, D. M. (1995) in *Rapid Freezing, Freeze-fracture and Deep Etching* (Severs, N.J., and Shotton, D.M., eds) pp. 31–50, Wiley-Liss, NY
19. Burnell, E. E., Cullis, P. R., and de Kruijff, B. *(1980) Biochim. Biophys. Acta* **603,** 63–69
20. Pake, G. E., and Purcell, E. M. (1948) *Physiol. Rev.* **74,** 1184
21. Traikia, M., Langlais, D. B., Cannarozzi, G. M., and Devaux, P. F. (1997) *J. Magn. Reson.* **125,** 140–144
22. Bloom, M., and Thewalt, J. L. (1995) *Mol. Membr. Biol.* **12,** 9–13
23. Seelig, J. (1977) *Q. Rev. Biophys.* **10,** 353–418
24. Korchev, Y. E., Bashford, C. L., Pederzolli, C., Pasternak, C. A., Morgan, P. J., Andrew, P. W., and Mitchell, T. J. (1998) *Biochem. J.* **329,** 571–577
25. Palmer, M., Harris, R., Freytag, C., Kehoe, M., Tranum-Jensen, J., and Bhakdi, S. (1998) *EMBO J.* **17,** 1598–1605
26. Bhakdi, S., and Tranum-Jensen, J. (1985) *Infect. Immun.* **48,** 713–719
27. Wright, J. K., Tschopp, J., Jaton, J.-T., and Engel, J. (1980) *Biochem. J.* **187,** 775–780
28. Aguillar, L., Ortega-Pierres, G., Campos, R., Fonseca, R., Ibánez, M., Wong, C., Farfán, N., Naciff, J. M, Kaetzel, M. A., Dedman, J. R., and Baeza, I. (1999) *J. Biol. Chem.* **274,** 25193–25196